Adaptive position–pressure control of a brake by wire actuator for sport motorcycles

Fabio Todeschini *, Matteo Corno, Giulio Panzani, Sergio M. Savaresi

Dipartimento di Elettronica, Informazione e Bioingegneria, Politecnico di Milano, Piazza L. da Vinci, 32, 20133 Milan, Italy

Received 17 July 2013
Accepted 19 December 2013
Recommended by L. Menini
Available online 3 January 2014

1. Introduction and motivation

The braking maneouver is one of the most critical and important situation that a vehicle undertakes, since it is intimately related to safety issues. Moreover, braking plays a fundamental role in sport/racing competitions. Not surprisingly, among the many applications of electronic vehicle dynamic control, the Anti-locking Braking System (ABS) was one of the first developed systems (the first automotive ABS-equipped vehicle appeared in 1954).

The four-wheeled vehicle area is rich of examples of control strategies aiming at improving the vehicle deceleration. The fundamental issue is preventing the wheel over-slippage or, even worse, the wheel locking that causes a loss of braking and steer performance. Some of the most interesting examples can be found in [4,16,9,1].

From the control design view-point there is a huge difference between motorcycle and automobiles. First of all this is due to economical and cultural reasons; the former can be easily understood by considering the small motorcycle market, compared to the four-wheeled vehicle. The latter is related to the fact that motorcycles have been considered as recreative vehicles for a long time, where electronic devices were usually seen as restrictions to the driving entertainment. The existing scientific literature points to another important factor, namely the complexity of motorcycle dynamics. In fact, besides the key issue of controlling the wheel slip, a motorcycle braking control system has to deal with other problems. The first one is the lateral instability of single-track vehicles that require the development of precise strategies: for example in [18,8,7] a curve-safe anti-lock braking system has been studied to prevent vehicle lateral instability during a curve panic brake maneouver. Another crucial aspect of motorcycle dynamic is the vehicle high centre of gravity (COG) position combined with a moderate wheelbase, which makes load transfer phenomena outstanding (compared to four-wheeled vehicles), significantly reducing the braking capability of the rear wheel. In [17,11,15] and in particular in [3] the role of the rear wheel brake, usually neglected, has been highlighted in the motorcycle optimal braking maneouver definition. For this reason, in [5] a gain-scheduled rear-wheel slip regulation that accounts for the vehicle load transfer has been developed.

Another important issue that has limited the spread of electronic braking control in motorcycles has been the lack of a consolidated technology for controlling the braking pressure. Motorcycle applications are highly demanding, since weight and packaging constraints are more severe than in four-wheeled vehicles. Recently, in [6] an innovative braking control architecture, devoted to single-track vehicle applications, has been presented and applied to the rear wheel of a motorcycle. This technology follows the *smart actuator* philosophy; *i.e.* an actuator that automatically tracks a reference profile. In particular, this actuator is based on the concept of hydraulically decoupling the driver braking command and the braking action itself, though exploiting the traditional hydraulic architecture of motorcycle brakes. Fig. 1 shows a pictorial representation of this system. The entire braking process is governed by the ECU; the driver braking request is acquired and processed by the control unit which

* Corresponding author.
E-mail address: todeschini@elet.polimi.it (F. Todeschini).

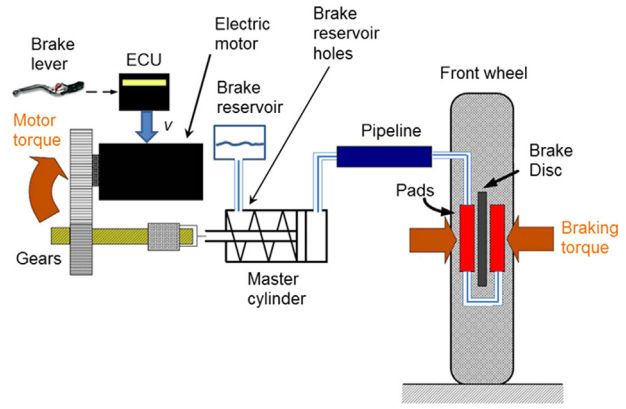

Fig. 1. A schematic representation of the BBW system.

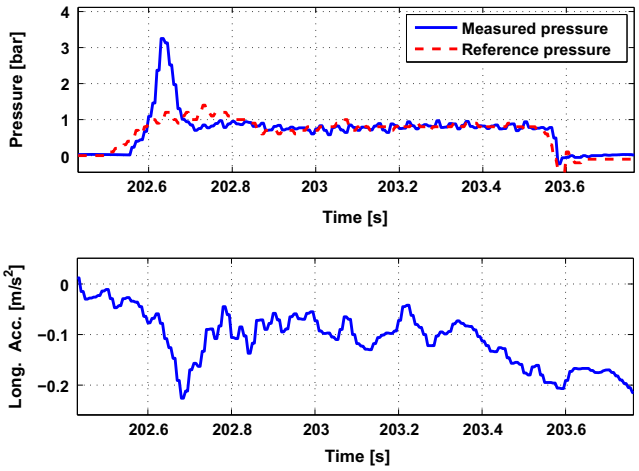

Fig. 2. Example of a motorbike deceleration caused by an overshoot in the pressure.

generates the command for the braking actuator according to the specific control law. The control action is computed starting from the available measurements, *i.e.* from the pressure in the master cylinder and its position.

The availability of such an actuator enables the smooth modulation of the braking torque. Thus, it can be used to develop vehicle control strategies such as racing ABS or vehicle stability control. With these goals, it is important to underline the control problem criticality: the pressure response must be fast enough and the robustness in every situation is crucial. More precisely, a closed-loop bandwidth of at least 10 Hz is required. Moreover, any pressure overshoot must be avoided, in fact, it causes an undesired deceleration in the vehicle. This may not be a problem when the motorbike is going straight, but, since the actuator is installed on the front wheel of a sport motorbike, it may result in a fall during a curve.

For example, Fig. 2 represents a fine braking modulation (average deceleration around 0.1 m/s^2). In that braking, a badly tuned controller causes an overshoot in pressure (top figure). The overshoot causes a negative peak in the longitudinal acceleration. Since this is a typical braking when the pilot tries to control the vehicle while steering, such a behaviour is unacceptable.

The actuator, due to its components, shows a non-linear behaviour. In [6] a control law is proposed, but the regulator design has been done without considering the just mentioned non-linearity. Instead, in this paper, we present a control architecture, based on the switching between a position and a pressure controller that takes into consideration the intrinsic system non-linearity. It is important to note that one could think to exploit the classical cascade architecture applied for such a system: a pressure controller that generates a position reference that feeds a position controller. The problem in this case is that increasing the position loop bandwidth over 10 Hz is very difficult. The cascade architecture requires the inner loop (in this case the position loop) to be decoupled from the outer loop (pressure control). Practitioners suggest at least a 10-fold difference in a closed-loop bandwidth. Because of sensing and actuation limit such a requirement cannot be satisfied by the position controller. For this reason, the position–pressure switching control is proposed. In addition, the system response is very affected by temperature variations and brake pad wear, so it can be considered as a time varying system. For this reason an adaptation algorithm is added to the control law in order to make the system robust to wear and varying conditions. The proposed control algorithm has been tested on a real circuit and experimental data are provided.

Firstly, the system architecture and the experimental setup are described (Section 2), then in Section 3, starting from physical equations governing every component, a mathematical model is derived. The model analysis is the starting point of the control strategy proposed in Section 4, where a hybrid position–pressure controller is presented. In particular, a position and a pressure controller are separately designed and a proper switching rule is derived. The main idea of the proposed control law is to use the position controller in the first part of the braking, then to switch to the pressure control. In Section 5 an adaptive algorithm which enhances the robustness of the closed loop system in terms of temperature variations and brake pad wear is presented. In Section 6 the controller proposed is experimentally validated. In particular, the controller response is evaluated in two different typical brakings. Final considerations are exposed in Section 7.

2. System description and experimental setup

The hardware actuator architecture used in this paper is the same electro-hydraulic brake by wire (BBW) firstly presented in [6]. A sport motorbike is equipped with this actuator. In particular, it is connected to the front brake caliper. A schematic portrait of the overall system is depicted in Fig. 1: the actuator is made up of an ECU, a DC motor, a gearbox and a ball screw capable of converting the motor rotative motion into a linear displacement, used to move the master cylinder piston, generating the pressure inside the hydraulic brake. The ECU has a microprocessor where the control logic is implemented. It is configured in order to have two different routines: the slow one ($f_{slow} = 200$ Hz) and the fast one ($f_{fast} = 1$ kHz). The ECU controls the voltage (v) applied to the motor.

Available system measures are as follows:

- motor current (i);
- engine rotation (θ). It is measured by an incremental Hall-effect encoder that can be converted in the linear displacement of the master cylinder piston (x), thanks to the gearbox ratio (η_g). The encoder resolution is 16 impulses per revolution, corresponding, in terms of the master cylinder position, to 0.125 mm;
- pressure in the master cylinder (p).

The presence of the return spring in the master cylinder guarantees the return of the piston to its rest position during zero pressure request (no actuation); this is a technological constraint and it cannot be removed or reduced. The brake reservoir carries out a fundamental role: when there is no braking, the master cylinder must retract enough to open the brake reservoir holes: in this way, the fluid flows in the reservoir compensating variation of fluid density due to temperature and pipeline volume due to brake pad wear.

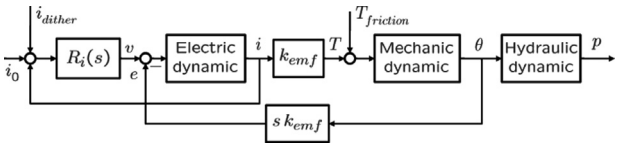

Fig. 3. BBW system equivalent block scheme.

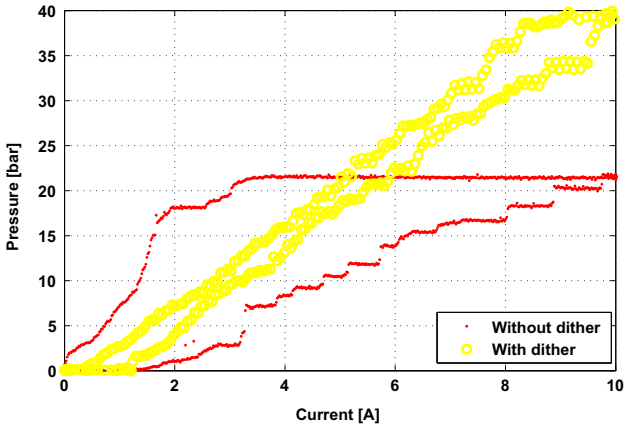

Fig. 4. Effect of dithering in reducing the static friction effect (hysteresis and stick and slip).

From now, we assume that an inner current control loop (with bandwidth ≈ 100 Hz) is present; since the current is proportional to the torque generated by the motor, this last variable can be considered as the actual input to the system. Fig. 3 depicts a functional block scheme of the considered system. It is affected by a significant friction force (represented by the equivalent torque $T_{friction}$); to remove its effect – at least the static Coulomb friction – a dithering signal (i_{dither}) is exploited. As discussed in [12–14], since friction depends on the braking pressure, the dither amplitude is scheduled on the pressure. To appreciate the benefits of this solution, Fig. 4 shows the current–pressure static map, with and without the dithering signal, when a slow current ramp is applied ($0 \rightarrow 10$ A in 10 s). When the dithering is used, it can be seen how the hysteresis and *stick and slip* phenomena can be reduced.

3. System modelling and identification

In this section the modelling of the complete hydraulic system is addressed. According to [10,6,2], a complete model of the overall system is described by the following equations:

$$\begin{cases} \dot{\theta} = \Omega \\ \dot{i} = \dfrac{Ri - v + k_{emf}\Omega}{L} \\ \dot{\Omega} = \dfrac{1}{J^*}(-k_p p_{mc} - k_{fr}F_{fr} + T) \\ \dot{p}_{mc} = \dfrac{\beta_e(p_{mc},R)}{V(\theta)}\left(\dfrac{p_{pd}-p_{mc}}{K_{lf}} + k_\Omega \Omega\right) \\ \dot{p}_{pd} = K_{pd}\dfrac{p_{mc}-p_{pd}}{K_{lf}} \end{cases} \tag{1}$$

with

$$\beta_e(p,R) = \beta \cdot \frac{R + \left(\dfrac{p}{p_{atm}}+1\right)^{1/\gamma}}{\dfrac{R}{\gamma}\dfrac{\beta}{p_{atm}+p} + \left(\dfrac{p}{p_{atm}}+1\right)^{1/\gamma}} \tag{2}$$

This model describes the open-loop behaviour of the system, considering the dynamic of all its elements. Ω is the angular velocity of the motor. The second equation accounts for the electric dynamic of the DC motor (modelled as an RL circuit) with the back EMF $k_{emf}\Omega$ and the voltage applied by the ECU v. The third equation represents the torque balance on the DC motor (with the equivalent rotational inertia J^* that comprises the inertia of gearbox and master cylinder): the motor torque T balances the force proportional to pressure and friction (both considered as equivalent torques, thanks to the coefficients k_p and k_{fr}). The fourth and the fifth equation describe the link between the pressure in the master cylinder and the pressure in the brake pads with the motion of the master cylinder piston: the volume V (function of the linear displacement x or angular rotation θ), the compressibility of the fluid (air + oil) $\beta_e(p_{mc},R)$, the coefficient that describes the laminar motion of the fluid inside the pipeline K_{lf} and the motion of the motor $k_\Omega\Omega$ are introduced to compute this link. The last equation computes the Bulk modulus [2], note that its value depends on the pressure and on the amount of the air in the fluid (R), *i.e.* on how the brake bleeding is done.

In a more control-oriented perspective, the following considerations can be done:

1. The presence of an inner current loop enables the decoupling between the electric and the mechanical part of the system.
2. The nominal working volume $\overline{V}$ can be considered constant, since variations due to piston position changes are negligible; thanks to this simplification, the influence of the first equation can be disregarded and the position of the master cylinder disappears from system's equations.
3. There is a high frequency dynamic (≈ 100 Hz, see [6]) that describes the relationship between the pressure in the master cylinder and the pressure in the pad; since the desired pressure closed loop bandwidth (≈ 10 Hz) is well beyond this frequency value, this dynamic can be disregarded.

Thanks to the previous simplifications, the model becomes a simpler second-order system:

$$\begin{aligned} \dot{\Omega} &= \frac{1}{J^*}(-k_p p_{mc} - k_{fr}F_{fr} + T) \\ \dot{p}_{mc} &= \frac{\beta_e(p_{mc},R)}{\overline{V}} k_\Omega \Omega \end{aligned} \tag{3}$$

The second equation of (3) represents the relationship between the pressure in the master cylinder and the piston position (or the motor angular position).

The experimental master cylinder position–pressure relationship is shown in Fig. 5 where $\partial p_{mc}/\partial x$ remains zero until a certain position, and then it increases with the position of the master cylinder. This is caused by the actuator physical configuration. In more detail, the system can be seen as a switching system that has three different configurations (see Fig. 5):

1. up to 1.4 mm the mechanical part is not connected to the hydraulic part, so any motor movement produces no pressure in the brake.
2. from 1.4 mm to 2.7 mm the mechanical part is connected to the hydraulic part, but the master cylinder is before the brake reservoir holes. For this reason, there is no (or at least very little) pressure increasing when the master cylinder moves forward.
3. from 2.7 mm the master cylinder is beyond the brake reservoir holes; hence, the hydraulic part is a close system and when the master cylinder compresses the fluid the pressure increases. Note that also in this part the position–pressure relationship is

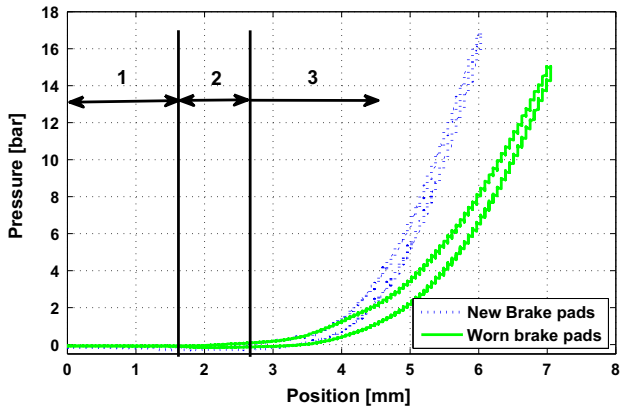

Fig. 5. Influence of brake pad wear highlighted with the three different system configurations in the position–pressure map.

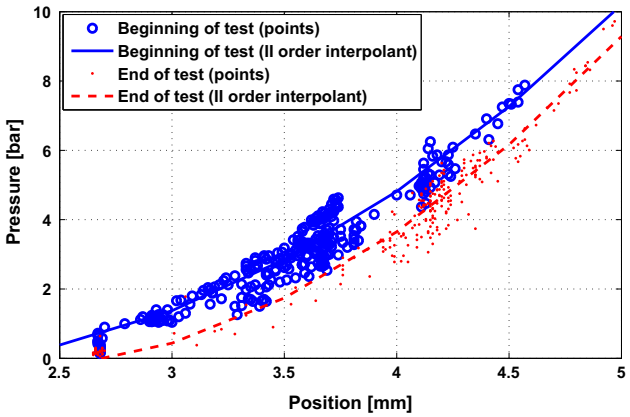

Fig. 6. Temperature effect (zoom in the third system configuration) in the position–pressure map.

not linear, this is caused by the Bulk modulus variations with the pressure.

The first two system configurations (up to 2.7 mm) establish the so-called *dead zone* in which any movement of the master cylinder piston does not produce any increase of pressure. The third configuration is the so-called *operative zone*, where the system is expected to work during its nominal usage. Note that there is no reason to bring the system in the mechanical *dead zone* (before 1.4 mm). This choice assures to minimize the space to cover when a brake request is done and to remain before the brake reservoir while waiting for a brake request.

In order to capture the system dynamics a black-box identification approach has been used. The control architecture proposed in this paper adopts two different controllers: a position controller and a pressure one. Two different input–output models will therefore be identified: current to pressure and current to position.

Regarding the current to pressure model identification problem, the system has been fed with a multi-frequency sinusoidal current (also known as *sweep*) from 1 Hz to 30 Hz with an increasing amplitude. To account for the effect of the bulk modulus variations, the identification has been done in several working conditions. The current and the pressure measurement are employed to compute the experimental system transfer function $\hat{G}_k(j\omega)$ according to the following expression [19]:

$$\hat{G}_k(j\omega) = \frac{\hat{S}_{p,k}(j\omega)}{\hat{S}_{i,k}(j\omega)} \tag{4}$$

where $\hat{S}_{p,k}(j\omega)$ represents the identified pressure spectrum in the working point k and $\hat{S}_{i,k}(j\omega)$ represents the identified current spectrum in the working point k.

In Fig. 7 the results of the current → pressure identification are depicted, where how the transfer functions change with the working point considered can be seen.

The current → position transfer function identification follows a path similar to the one just presented, the only substantial difference lies in the poor position resolution measure. For that, in order to make the system moving around an equilibrium point, we did not feed the system with a continuous sweep, but identification has been done point by point in the frequency domain. The current → position transfer function identification has been done in the *dead zone* and the *operative zone* ($p = 10$ bar). Note that with the control architecture here presented (Section 4), the position control will mostly work in the *dead zone*, so the identification in this area is fundamental. The identification in the *operative zone* has been done to check if a fixed structure controller can provide satisfactory performances in both configurations. The experimental points found are depicted in Fig. 8,

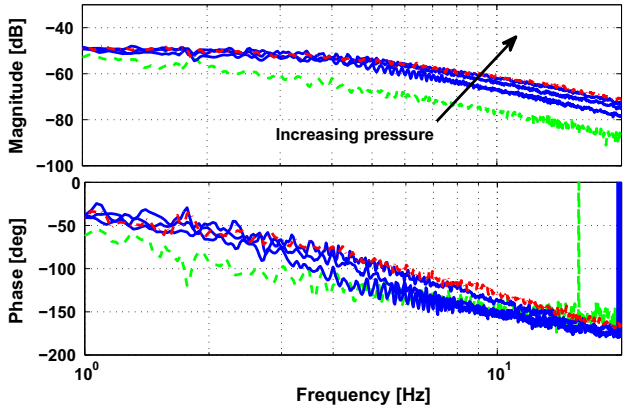

Fig. 7. Experimental current–pressure transfer functions.

where the transfer functions that approximate the experimental points are also shown. Note that the identified transfer functions are different until 5 Hz, than they converge, this would suggest to use a fixed structure controller that guarantees a closed loop bandwidth greater than 5 Hz.

Due to the temperature effect, the brake pads wear and the high friction present in the system, the model is heavily affected by uncertainties. Fig. 5 shows how the relationship between position and pressure changes with the brake pads wear. This is not surprising since, due to the wear, the volume $\overline{V}$ of the fluid in the hydraulic part increases and so, from the second equation in (3) it can be seen that $\dot{p}_{mc}$ decreases. Basically, with worn brake pads, given a certain master cylinder position the pressure is lower than the one obtained with new brake pads. Temperature influences the position–pressure relationship as well. In Fig. 6, the comparison between position and pressure points can be evaluated when the system is cold (*i.e.* at the first braking) and when the system reaches the regime temperature (*i.e.* after a certain number of braking).

4. Control law design

In this section a controller is proposed. Firstly, the robustness of a pressure only controller will be discussed and a simple PID regulator with lead compensator will be tuned, proving sufficiently robust with respect to system variations in the *operating zone*. Then, to improve the performances obtained with the pure

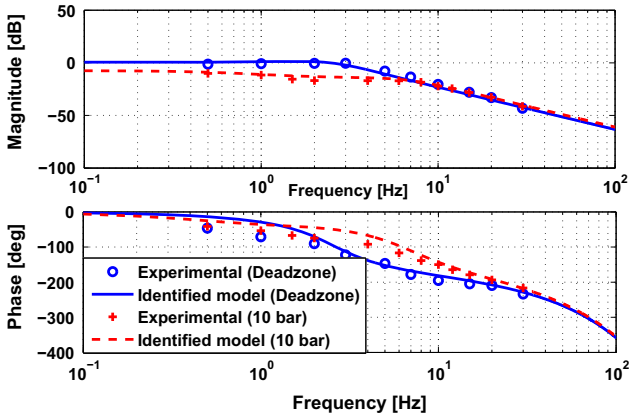

Fig. 8. Identified current–position transfer functions.

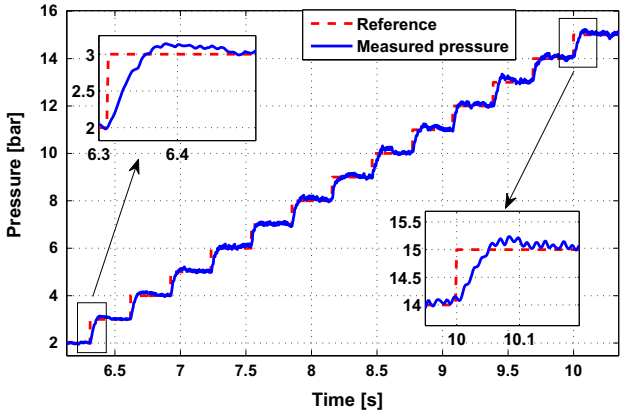

Fig. 9. Experimental performances on small step reference variation (1 bar amplitude) of the pressure controller.

pressure controller, the position measure will be exploited. The principle relies on the switching between two different controllers. At the beginning of the brake, while the system moves in the dead zone, the position controller is used since the pressure is uncontrollable; then, once the system approaches the desired working point, the pressure controller is activated in order to precisely track the pressure target.

4.1. *Pressure control*

The pressure controller is designed based on the identification results shown in Fig. 7. The system dynamics around 10 Hz – that is the desired closed loop bandwidth – exhibit a strong dependence on the working point. For this reason the following strategy has been adopted: a PID controller has been tuned considering a nominal system in the *operating zone*, around 10 bar pressure. To face the loss of phase due to a lower pressure operating point, a lead compensator has been added. Fig. 9 shows the performances of the proposed controller in response to small step reference variation. It can be observed how the pressure reaches the reference after about 60 *ms* and there is an admissible overshoot. This happens not only in the working point where the controller has been tuned (high pressure) but also for low pressure, so in the worst condition that it could operate in. This demonstrates the robustness of the pressure control with respect to the operating point.

When testing the closed loop system with high amplitude reference signals (as for example shown in Fig. 10), it turns out that the tracking results are not as satisfactory as expected. The upper panel shows the pressure controller step response, starting from null pressure (*i.e.* from x = 1.4 mm): a significant delay and a 33% overshoot can be noted. This is due to the fact that while the piston crosses the *dead zone* there is no increase of pressure. During this equivalent delay the integral part of the controller significantly augments the value of the control action causing the overshoot. The initial *dead zone* is not the only issue. The lower panel of Fig. 10 shows a 7 bar step response starting from 1 bar. In this case the controller tuned on the identified system does not deliver the required performance, too.

In sport motorbikes, the first part of the braking is the most critical one: usually the pilot strongly presses the brake lever, then, after the motorbikes starts to decelerate, he slowly modulates. For this reason, from a control perspective, at the beginning of the braking the master cylinder must cross the *dead zone* and reach a pressure with the minimum tracking delay. It is easy to understand that, adopting just a pure pressure controller, the problems shown in Fig. 10 would cause a bad feeling on the vehicle. In other words, the pilot will feel the overshoot effect and this can be dangerous, especially during a curve.

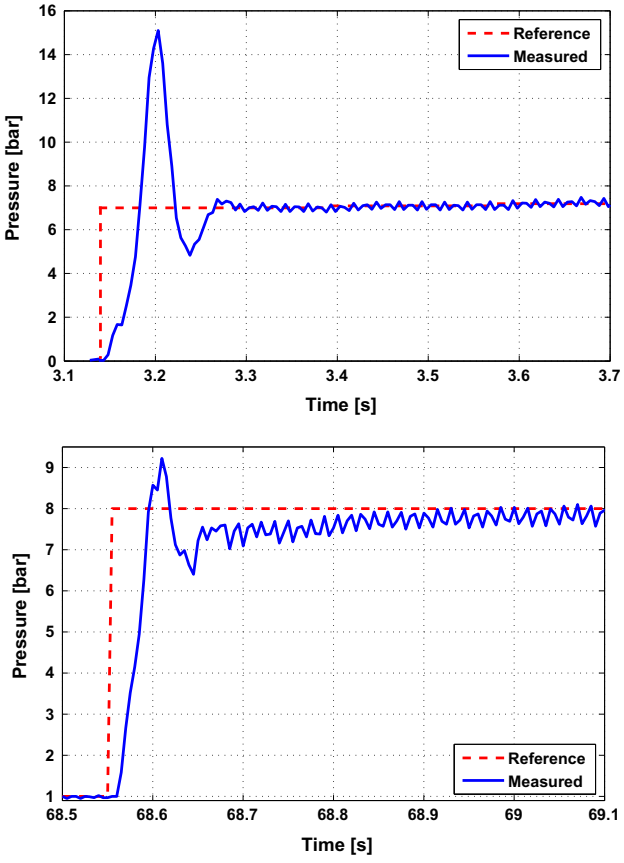

Fig. 10. *Dead zone* effect (top plot) and large step response (bottom plot).

4.2. *Position–pressure hybrid control*

To solve the aforementioned problems, the main idea is to use a position controller to quickly bring the system around the working point; then the controller switches to a pressure control to ensure a precise tracking of the desired pressure. Thus, the proposed control architecture (Fig. 11) has two different controllers (position and pressure) that work alternatively.

A finite state machine supervises the proper switching between regulators: the automaton is pictorially represented in Fig. 12. The state of the FSM are as follows:

- `Idle`: The position controller is enabled in order to maintain the system right before the beginning of the brake reservoir but after the mechanical *dead zone*. To do so, the position reference is set equal to 1.4 mm.
- `Position control – dead zone`: The position controller is enabled in order to bring the master cylinder in the minimum time after the brake reservoir. In this case, the position reference is set equal to 2.7 mm.
- `Position control – operative zone`: The position controller is enabled in order to bring the system to a point where the pressure is close to the requested one. In this phase the position reference is computed from the pressure one through inverting the position–pressure map. The estimation algorithm proposed in Section 5 will be able to provide a recursively updated pressure–position map. This guarantees the right position reference computation throughout the actuator functioning.
- `Pressure control`: Pressure control is enabled.

As it can be seen from Fig. 12, the transition from `Idle` to `Position control – dead zone` is activated when the pressure reference is greater than zero. The state of the FSM remains there until the master cylinder is almost after the brake reservoir ($x > x_{rif} \cdot 0.9$). The transition between `Position control – dead zone` and `Position control – operative zone` is activated with the same condition as before ($x > x_{rif} \cdot 0.9$), but in this case the position reference is generated from the pressure one through inverting the position–pressure map. `Pressure control` remains enabled until the pressure reference returns zero. In order to guarantee a bumpless switch between the two controllers, the not-working controller is fed with a reference equal to the inactive measured variable.

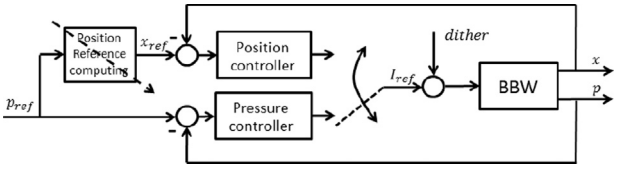

Fig. 11. Proposed hybrid position–pressure controller architecture.

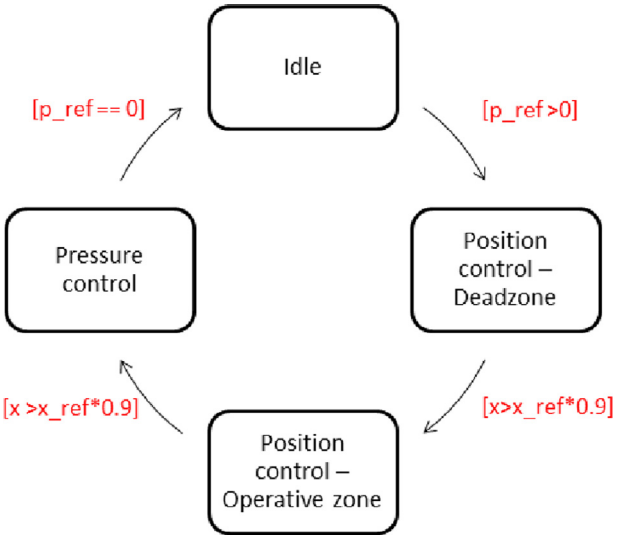

Fig. 12. Finite state machine that supervises the switch between the pressure and position controllers.

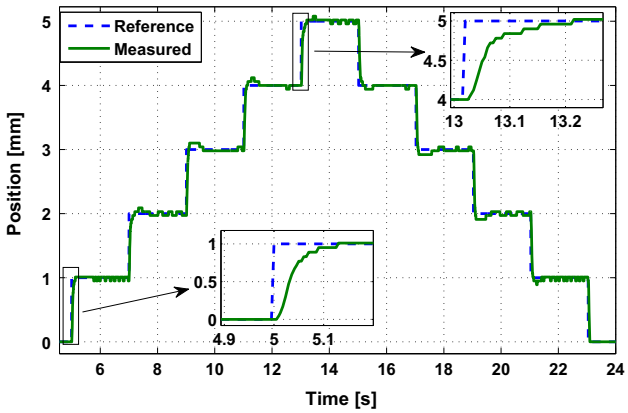

Fig. 13. Experimental performances of the closed loop position control in every possible working.

Like the pressure controller, the position one must be tuned in order to obtain a closed loop bandwidth of 10 Hz; this is done based on the identified transfer functions shown in Fig. 8. Focussing on how the position controller will be used in the proposed control strategies, it is clear that the controller will mostly work in the *dead zone*. The position controller is then designed considering the transfer function identified in that area. It is also important to notice that the transfer function in the *dead zone* and the one in the *operative zone* are very similar for frequency greater than 5 Hz, so good performances are expected in the *operative zone* too.

Fig. 13 shows the position closed-loop performances; it can be appreciated how the response time is about 100 ms in the *dead zone* and it slightly increases in the *operative zone*. However, adopting a fixed structured controller, closed-loop performances are not significantly affected by changes in the working point and there is no overshoot in the response.

5. Position–pressure curve estimation

As mentioned before, the position–pressure relationship is varying with respect to temperature and brake pad wear. Since the position reference is computed exploiting this curve, an adaptation algorithm needs to be adopted. The goal of the adaptation algorithm is to collect the position–pressure points and to find a curve fitting that matches the position–pressure curve. The pressure can be approximated as a second-order polynomial as follows:

$$\hat{y}(t) = \phi_E(t)^T \cdot \hat{\theta} = [1 \;\; x(t) \;\; x(t)^2] \cdot \begin{bmatrix} c \\ b \\ a \end{bmatrix} \tag{5}$$

where $x(t)$ represents the position measured at the time t. a, b and c are the unknown parameters that the adaptation algorithm aims at estimating.

Thus, the estimation error can be computed as follows:

$$\varepsilon(t) = y(t) - \hat{y}(t). \tag{6}$$

The estimation problem is linear in the parameter. In order to minimize the computational time avoiding the matrix inversion, Extended Least Square (ELS, Eq. (7)) has been adopted:

$$\begin{cases} \hat{\theta}_t = \hat{\theta}_{t-1} + K(t)\varepsilon(t) \\ K(t) = V(t)\phi_E(t) \\ V(t) = V(t-1) - \beta_{t-1}^{-1} V(t-1)\phi_E(t) \cdot \\ \quad \cdot \phi_E(t)^T V(t-1) \\ \beta_{t-1} = 1 + \phi_E(t)^T V(t-1)\phi_E(t) \end{cases} \tag{7}$$

Note that Eqs. (7) are recursive, and $V(t)$ is initialized as follows:

$$V(0) = \alpha \cdot I \tag{8}$$

where $\alpha > 0$. It is also important to note that $V(0)$, except for a multiplicative term, represents the initial variance of the unknown parameters $\hat{\theta}(0)$.

The position control is performed just in the first part of the braking, so the knowledge of the exact position–pressure map is important only in this phase. Also, the first part of the position–pressure map does not change (mechanical *dead zone* and brake reservoir), so changing due to wear and temperature is visible when the master cylinder is after the brake reservoir. For this reason, we decided to switch on the estimation algorithm when the FSM is in the `Position control – operative zone`. For numerical reasons, the algorithm has to be switched off when the input is not exciting the system, otherwise, it will diverge. So, at the end of the braking, it will be switched off. The new estimated parameters are updated at the end of the braking; in this way, when a new braking happens the updated position–pressure curve is available. Fig. 6 plots position–pressure points when the brake is cold and when it is at the regime temperature. On-line estimated curves with ELS are depicted too.

6. Experimental results

A sport motorbike equipped with the described brake by wire actuator has been tested on a real circuit by a professional driver. The pressure reference is generated according to the front brake lever, then sent to the brake by wire actuator.

In Fig. 14, the tracking performances are evaluated in a slight braking, *i.e.* where the reference pressure increase rate is small (almost 2 bar/s). The main plot shows pressure and speed during the entire braking; in the small bottom plot a zoom of position and pressure in the first part of the braking is provided. As can be seen in the small plot, the actuator is in the idle position at the very beginning ($x = 1.4$ mm, switching signal = 0), when the pressure reference becomes greater than zero, the position reference becomes 2.7 mm (switching signal = 1), when the master cylinder overcomes the brake reservoir, the position reference is computed from the pressure one (switching signal = 2). According to the finite state machine (Fig. 12), when the master cylinder position reaches almost the position reference ($x > x_{ref} \cdot 0.9$), the pressure control is enabled (switching signal = 3). This state remains until there is no braking request, when the system goes back into the idle position.

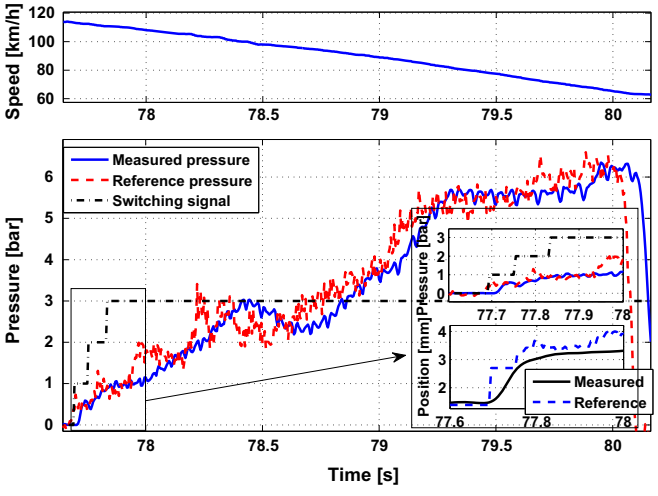

Fig. 14. Experimental tracking results on a motorbike. Complete pressure tracking and zoom about the most critical part in a slight braking.

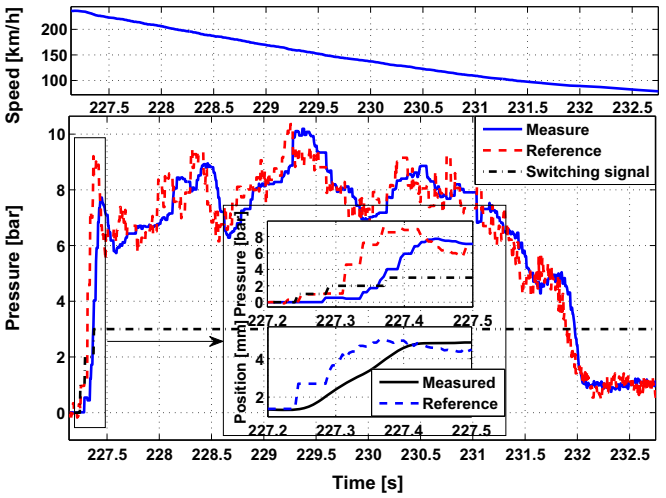

Fig. 15. Experimental tracking results on a motorbike. Complete pressure tracking and zoom about the most critical part in a strong braking.

Similar to the previous figure, in Fig. 15 the tracking performance in a strong brake is depicted. The reference pressure increase rate is greater than before (almost 100 bar/s) and after the first strong part, the pilot modulates the braking. Focussing on the first part, it can be seen that the control evolution is the same as before: the master cylinder overcomes the brake reservoir, then control remains in the position tracking until the position reference is almost reached. At this point pressure control becomes active. It is worthy to note that in this case, when switching from position control to pressure control (switching signal 2→3) the pressure is not exactly the one expected from the position–pressure map. This is caused by the position–pressure map dispersion, however, the position control gives contribution that avoids the overshoot shown in Fig. 10. Also, Figs. 14 and 15 show how the time response is less than 80 ms, equivalent to a 10 Hz closed loop bandwidth.

Usually, the most critical phase for the control algorithm is the first laps, when the brake starts from being cold to the regime temperature. We did tests with and without the adaptation algorithm in order to prove the effectiveness of the adaptation. Fig. 16 plots the Root Mean Square of the tracking error per lap, when the adaptation algorithm is on, RMS does not change significantly. Instead, when testing the control law without the adaptation algorithm (so with the position–pressure map identified at the beginning of the test and kept constant during the test), RMS becomes four times greater from the first lap to the second one. With the adaptation off, after two laps, the tests were stopped because of a bad pressure tracking, that is why there is no data available for the third lap in this experiment. The bad tracking is caused by an imprecise position reference and when switching to the pressure control, the pressure manifests the problems depicted in Fig. 10.

In conclusion, the adaptation algorithm is able to adapt the position–pressure map guaranteeing consistent tracking performances. In other words, the adaptation algorithm makes the control law robust with respect to temperature variations and brake pad wear.

7. Conclusion

In this paper the control of an innovative electro-mechanical brake-by-wire actuator has been presented. In particular, the importance of the nonlinearities, summarized in the nonlinear master cylinder piston position–plant pressure map, has been

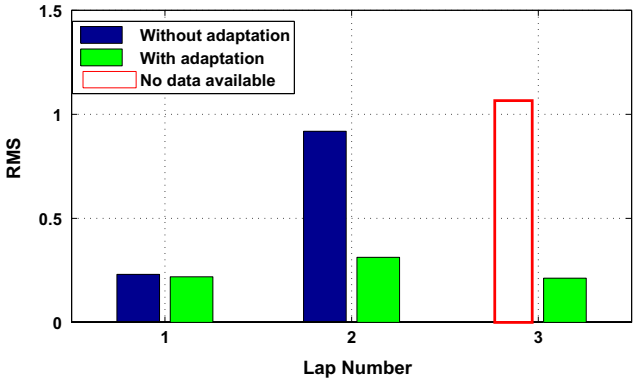

Fig. 16. Root Mean Square error per lap with and without the adaptation algorithm.

highlighted. A control oriented model has been derived: simple but capable of capturing the most important aspects in the pressure control problem. The physics-based analysis of the system has underlined the importance of having a position controller that brings the master cylinder after the brake reservoir, where the pressure is controllable. Also, the position controller brings the system around the pressure working point, where the pressure controller has good performances. A finite state machine that supervises the position and pressure controllers has been presented. In order to have a control logic robust with respect to the temperature effect and the brake pad wear, an adaptation algorithm has been introduced. Experimental results have shown that the required performances are achieved and the effectiveness of the adaptation algorithm has been successfully tested.

References

[1] Y. Chin, W. Lin, D. Sidlosky, D. Rule, M. Sparschu, Sliding-mode ABS wheel-slip control, in: American Control Conference, IEEE, 1992, pp. 1–8.

[2] B.-H. Cho, H.-W. Lee, J.-S. Oh, Estimation technique of air content in automatic transmission fluid by measuring effective bulk modulus, Int. J. Automot. Technol. (2002) 57–61.

[3] M. Corno, S. Savaresi, M. Tanelli, L. Fabbri, On optimal motorcycle braking, Control Eng. Pract. 16 (6) (2008) 644–657.

[4] M. Corno, S. Savaresi, G. Balas, On linear-parameter-varying (LPV) slip-controller design for two-wheeled vehicles, Int. J. Robust Nonlinear Control 19 (12) (2009) 1313–1336.

[5] M. Corno, M. Tanelli, S. Savaresi, L. Fabbri, L. Nardo, Design and validation of a gain-scheduled controller for the electronic throttle body in ride-by-wire racing motorcycles, IEEE Trans. Control Syst. Technol. (2011) 1–13.

[6] A. Dardanelli, G. Alli, S. Savaresi, Modeling and control of an electro-mechanical brake-by-wire actuator for a sport motorbike, in: Mechatronic Systems, 2010, pp. 524–531.

[7] B. Hauser, H. Ohm, G. Roll, Motorcycle ABS using horizontal and vertical acceleration sensors, US Patent 5,445,443, August 29 1995.

[8] M. Hirsch, D. Alberer, L. del Re, Stability control by advanced full-braking systems of motorbike vehicles, in: ASME 2006 International Mechanical Engineering Congress and Exposition, ASME, 2006.

[9] T. Johansen, I. Petersen, J. Kalkkuhl, J. Ludemann, Gain-scheduled wheel slip control in automotive brake systems, IEEE Trans. Control Syst. Technol. 11 (6) (2003) 799–811.

[10] Y. Khan, P. Kulkarni, K. Youcef-Toumi, Modelling experimentation and simulation of a brake apply system, in: American Control Conference, IEEE, 1992, pp. 226–230.

[11] D. Limebeer, R. Sharp, S. Evangelou, The stability of motorcycles under acceleration and braking, Proc. Inst. Mech. Eng. Part C: J. Mech. Eng. Sci. 215 (9) (2001) 1095–1109.

[12] M. Michaux, A. Ferri, K. Cunefare, Effect of tangential dither signal on friction induced oscillations in an SDOF model, J. Comput. Nonlinear Dyn. 2 (2007) 201.

[13] H. Olsson, K. Åström, C. Canudas de Wit, M. Gäfvert, P. Lischinsky, Friction models and friction compensation, Eur. J. Control 4 (1998) 176–195.

[14] G. Panzani, M. Corno, S. Savaresi, On adaptive electronic throttle control for sport motorcycles, Control Eng. Pract. 21 (1) (2013) 42–53.

[15] G. Panzani, S. Formentin, S. Savaresi, Active motorcycle braking via direct data-driven load transfer scheduling, in: 16th IFAC Symposium on System Identification, SYSID 16 (1) (2012) 1257–1262.

[16] S. Savaresi, M. Tanelli, C. Cantoni, Mixed slip-deceleration control in automotive braking systems, J. Dyn. Syst. Meas. Control 129 (2007) 20.

[17] R. Sharp, Limit braking of a high-performance motorcycle, Veh. Syst. Dyn. 47 (5) (2009) 613–625.

[18] M. Tanelli, M. Corno, I. Boniolo, S. Savaresi, Active braking control of two-wheeled vehicles on curves, Int. J. Veh. Auton. Syst. 7 (3) (2009) 243–269.

[19] P. Wellstead, Non-parametric methods of system identification, Automatica 17 (1) (1981) 55–69.